Research Article Vol. 14, No. 8 / 1 Aug 2024 / Optical Materials Express 2083
Optical Materials EXPRESS

Enhancement of the environmental stability of perovskite thin films via AZ5214-photoresist and PMMA coatings

KIMYA FALLAH,[1] SHAHAB NOROUZIAN ALAM,[1,2] BIJAN GHAFFARY,[1] FARZANEH YEKEKAR,[1] SHIMA TAGHIYAN,[1] AND SAJJAD TARAVATI[3,*]

[1]Physics Department, Iran University of Science and Technology, Tehran, Iran
[2]Optoelectronics Research Center, Iran University of Science and Technology, Tehran, Iran
[3]School of Electronics and Computer Science, University of Southampton, Southampton, SO17 1BJ, UK
[*]S.Taravati@soton.ac.uk

Abstract: This study presents a novel investigation into enhancing the environmental stability of perovskite thin films, specifically focusing on the effects of AZ5214 photoresist compared to the widely studied PMMA. By employing advanced matrix encapsulation techniques, we aim to stabilize methylammonium lead iodide ($MAPbI_3$) and methylammonium lead bromide ($MAPbBr_3$) films, which are meticulously prepared via a two-step solution deposition method under controlled ambient conditions. Our approach involves spin-coating layers of poly(methyl methacrylate) (PMMA) and AZ5214 photoresist to singularly encapsulate the perovskite films. This encapsulation provides a robust hydrophobic barrier, significantly mitigating moisture ingress and addressing pinhole challenges within the perovskite structure. Through comprehensive characterizations—including scanning electron microscopy (SEM), X-ray diffraction (XRD), and photoluminescence (PL) spectroscopy—we demonstrate that AZ5214 photoresist, despite being thicker than PMMA, offers significantly enhanced stability. Our study revealed that coating $MAPbI_3$ perovskite with a 127-nanometer layer of PMMA resulted in a PL intensity retention of 44.8% after 40 days, which is a 589.23% improvement over the uncoated perovskite. Similarly, a 1200-nanometer layer of AZ5214 photoresist achieved a PL intensity retention of 38.2%, reflecting a 487.69% enhancement. For $MAPbBr_3$ perovskite, the PMMA coating achieved a PL intensity retention of 43.1%, a 71.72% improvement, while the AZ5214 photoresist coating resulted in a retention of 48.4%, showing a 92.83% enhancement. These findings highlight the superior stability provided by AZ5214 photoresist, especially for $MAPbBr_3$, making it a more effective barrier against environmental degradation compared to PMMA.

1. Introduction

Lead halide perovskites (LHPs) have risen to prominence as exceptional optoelectronic materials, thanks to their superior photovoltaic power conversion efficiencies [1] and cost-effective production [2]. They exhibit a crystalline structure similar to calcium titanium oxide ($CaTiO_3$), adopting the general formula ABX_3. In this formula, "A" represents a cation, such as methylammonium ($CH_3NH_3^+$), formamidinium ($CH(NH_2)_2^+$), or cesium; "B" denotes lead (Pb); and "X" is a halide anion, which can be chloride (Cl^-), bromide (Br^-), or iodide (I^-). These compounds are part of the wider perovskite material family, distinguished by their unique and adaptable crystalline framework. They boast impressive features, including long charge carrier diffusion lengths [3], precise tunable bandgaps [4], high light absorption coefficients [5–7], electronic correlations and unusual excitonic effects [8], and exceptional defect tolerance [9]. The exceptional photovoltaic

#532998 https://doi.org/10.1364/OME.532998
Journal © 2024 Received 18 Jun 2024; revised 7 Jul 2024; accepted 23 Jul 2024; published 31 Jul 2024

Optical Materials EXPRESS

characteristics of these optoelectronic materials, as detailed in existing literature [1,10], position them as a highly promising foundation for the development of next-generation, high-frequency, dynamic metasurfaces [11–14]. In addition, LHPs are excellent candidates for creation of exciton polariton at room temperature thanks to their large exciton binding energy and quantum yield [15]. Such attributes make LHPs particularly well-suited for the fabrication of optoelectronic devices [16,17], solar cells [6,18–23], lasers [24], light-emitting diodes (LEDs) [10,25], quantum confinement and dielectric deconfinement [26], photovoltaic and photocatalysis applications [27], and detectors [28,29].

However, despite their immense potential, LHP materials face significant challenges when exposed to external factors such as moisture and heat, largely due to their minimal formation energy (approximately 0.1-0.3 eV) [30–32]. Enhancing the stability of perovskite materials is therefore crucial for extending the lifespan and performance of devices based on these materials [41,42]. Various methods have been explored to fortify LHPs against water ingress [33–35], yet many of these approaches can lead to the generation of surface lead ions and the formation of easily exfoliated coatings due to the presence of fragile chemical bonds [36]. To address these challenges, researchers have investigated the incorporation of poly methyl methacrylate (PMMA) onto LHP nano-crystals (NCs) [36–38]. The ester carbonyl groups of PMMA contribute to the formation of high-quality composite LHP films, characterized by pure colors and exceptional resistance to both heat and water [39].

In this study, we present an exploration into enhancing the stability of perovskite structures by applying nanostructured layers of AZ5214 photoresist and PMMA separately. We synthesize $MAPbI_3$ and $MAPbBr_3$ films with single-side layers of AZ5214 photoresist and PMMA individually. Structural and optical properties are systematically investigated using X-ray diffraction (XRD), photoluminescence (PL), and scanning electron microscopy (SEM). Our findings reveal that the utilization of the AZ5214 photoresist layer effectively shields the perovskite layer against environmental factors, demonstrating comparable performance to the PMMA layer in this regard.

2. Materials and methods

2.1. Materials

Glass slides (1×1 cm), lead iodide powder (PbI_2), methylammonium iodide powder (MAI), PMMA powder, acetone, methylammonium bromide powder (MABr), lead bromide powder ($PbBr_2$), dimethyl sulfoxide (DMSO), AZ5214 photoresist, and chlorobenzene were sourced from Merk company and utilized as received without additional purification. Scanning electron microscope XL300 manufactured by Philips. X-ray diffraction spectrometer Expert manufactured by Philips. Photoluminescence device Noora 200.

2.2. Synthesis of perovskite solution and PMMA polymer

Figure 1 demonstrates a schematic representation of the proposed solutions for enhancing the stability of $MAPbI_3$ and $MAPbBr_3$ perovskite structures by applying AZ5214 photoresist and PMMA coatings. The precursor solutions for $MAPbI_3$ and $MAPbBr_3$ were prepared by dissolving 55 mg of MAI (MABr) and 190 mg of PbI_2 ($PbBr_2$), respectively, with a 3:1 molar ratio in 300.5 μl of DMSO at 180°C. To ensure dehumidification, the lid of the PbI_2 ($PbBr_2$) vial (190 mg for PbI_2 and 181 mg for $PbBr_2$) was opened and placed on a hotplate at 100°C for 10 minutes, sealed, and then allowed to cool to ambient temperature. Subsequently, 300.5 μl of DMSO was added at 180°C and stirred until completely dissolved. The final precursor solution for $MAPbI_3$ ($MAPbBr_3$) was obtained by adding 55 mg of MAI (MABr) to 291 μl of the above solution, followed by chilling and continuous stirring for 5 minutes, as depicted in Fig. 2. For the

Optical Materials EXPRESS

preparation of the PMMA polymer solution, 25 mg of PMMA powder was dissolved in 500 μl of acetone by stirring for 30 seconds.

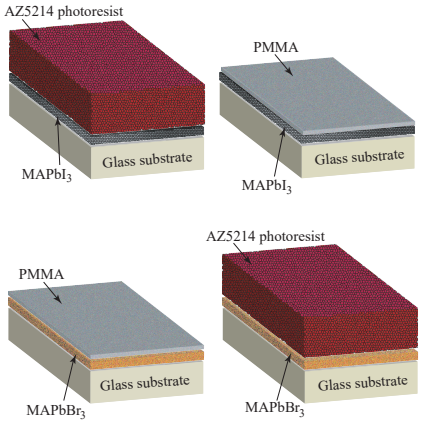

Fig. 1. Enhancing the stability of $MAPbI_3$ and $MAPbBr_3$ perovskite structures by applying AZ5214 photoresist and PMMA coatings.

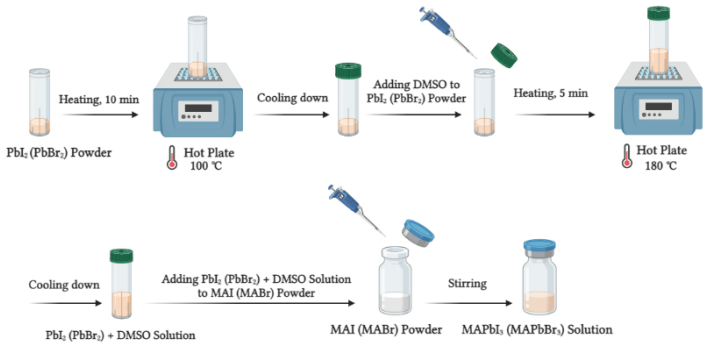

Fig. 2. Synthesis of $MAPbI_3$ and $MAPbBr_3$ solutions.

2.3. *Fabrication of perovskite thin film*

The glass substrates underwent a rigorous cleaning process involving sequential immersion in water and soap, double-distilled water, and ethanol, followed by ultrasonication at 70°C for 10 minutes after each step. Subsequently, the substrates were dried using a heat gun and then placed in a laboratory furnace at 500°C for one hour to ensure thorough drying.

To fabricate $MAPbI_3$ ($MAPbBr_3$) thin films, the spin-coating technique, specifically the nanocrystal-pinning (NCP) process, was employed in two steps. The cleaned substrate was mounted on a spin-coater, and 25 μl of $MAPbI_3$ ($MAPbBr_3$) precursor solution was dispensed onto it, followed by acceleration to 1000 rpm for 10 seconds and then to 4000 rpm for 30 seconds. At the 15-second mark of the second step, 100 μl of chlorobenzene solution was dispensed onto the spinning substrate. Subsequent evaporation of the remaining solution facilitated rapid crystallization of the perovskite nanocrystals (NCs). For additional annealing, the substrate was placed on a hotplate at 100°C for 40 minutes.

Once the film had cooled, a layer of PMMA polymer (or AZ5214 photoresist) was applied atop the perovskite layer. The spin-coating process was repeated, with acceleration to 3000 rpm

Optical Materials EXPRESS

(a) (b) (c)

Fig. 3. Images of $MAPbI_3$ perovskite samples: (a) Perovskite, (b) Perovskite with PMMA, and (c) Perovskite with AZ5214 photoresist.

(a) (b) (c)

Fig. 4. Images of $MAPbBr_3$ perovskite samples: (a) Perovskite, (b) Perovskite with PMMA, and (c) Perovskite with AZ5214 photoresist.

(6000 rpm for AZ5214 photoresist) for 30 seconds, followed by placement on a hotplate at 100°C for 10 minutes to ensure proper adhesion and drying. Representative samples are depicted in Figs. 3 and 4. The $MAPbI_3$ perovskite is typically brown due to the presence of iodine, while the $MAPbBr_3$ perovskite appears orange because of the bromine. The PMMA solution is transparent, so adding a PMMA layer does not change the color of the $MAPbI_3$ and $MAPbBr_3$ perovskite layers. On the other hand, the AZ5214 photoresist is a red solution. Therefore, when an AZ5214

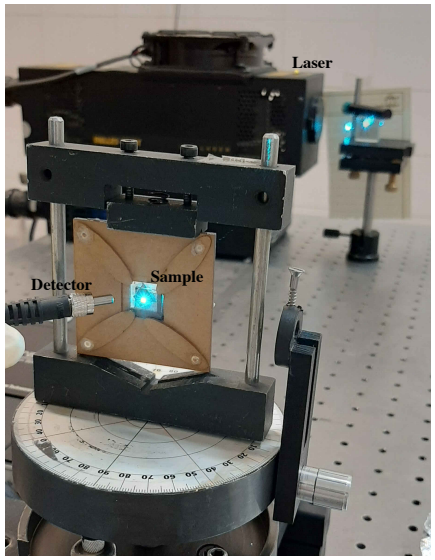

Fig. 5. SEM-Top images of the perovskite surface with (a) PMMA, and (b) AZ5214

Fig. 5. Experimental setup for photoluminescence (PL) spectroscopy.

Optical Materials EXPRESS

photoresist layer is applied to $MAPbI_3$ and $MAPbBr_3$ perovskite layers, it makes their colors slightly more intense. This slight change in color intensity is indicative of the strong interaction between the AZ5214 photoresist and the perovskite materials, which can further contribute to the improved stability and performance observed in our study. These color changes, while minor, highlight the successful application of the encapsulant layers and their role in enhancing the durability of the perovskite films.

2.4. Experimental setup

Figure 5 shows the experimental setup for photoluminescence (PL) spectroscopy. Due to limited access to XRD equipment, the earliest we can conduct XRD analysis is approximately 24 hours after sample deposition. To ensure the samples remain as fresh as possible for this 24-hour XRD analysis, we store them in a desiccator within a nitrogen-filled glovebox to maintain a vacuum-like environment. Therefore, we consider the XRD results obtained at 24 hours post-deposition to represent the fresh samples, while those obtained after 40 days are used to illustrate long-term stability.

3. Results

3.1. Morphological analysis of $MAPbI_3$ perovskite thin films using SEM

The morphology of the $MAPbI_3$ perovskite thin layer was investigated through SEM, including top-view (SEM-Top) and cross-sectional (SEM-Cross). Figures 6(a) to 6(c) present SEM-Top analysis results for the optimal perovskite layer at three different resolutions, that is, 50 μm, 5 μm and 1 μm.

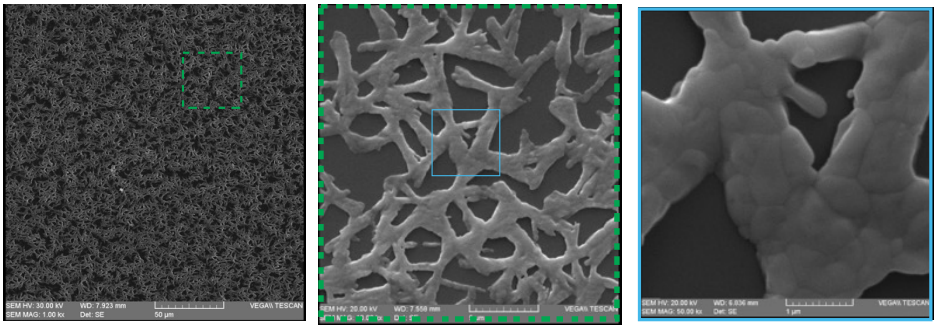

(a) (b) (c)

Fig. 6. SEM top images of the perovskite surface at three different resolutions. (a) 50 μm. (b) 5 μm. (c) 1 μm.

Figures 7(a) and 7(b) provide a comparative analysis of the SEM-Top images of the perovskite surface, perovskite with PMMA, and perovskite with AZ5214 photoresist. The application of PMMA and AZ5214 photoresist does not alter the inherent structure of the perovskite; instead, it serves to encapsulate the perovskite material, creating a protective layer akin to plastic. This encapsulation process enhances the stability of the perovskite against various environmental factors.

Figure 8(a) shows an SEM cross-sectional analysis of $MAPbI_3$ perovskite, with a thickness of 425 nanometers, deposited on a glass substrate. Figure 8(b) presents an SEM cross-sectional analysis of the same $MAPbI_3$ perovskite layer, now with an additional 127-nanometer PMMA layer deposited on top. Figure 8(c) displays an SEM cross-sectional analysis of the $MAPbI_3$ perovskite, again at 425 nanometers thick, with a 1200-nanometer AZ5214 photoresist layer applied on top. The thickness of each encapsulation layer was controlled using a precise spin-coating technique,

Optical Materials EXPRESS

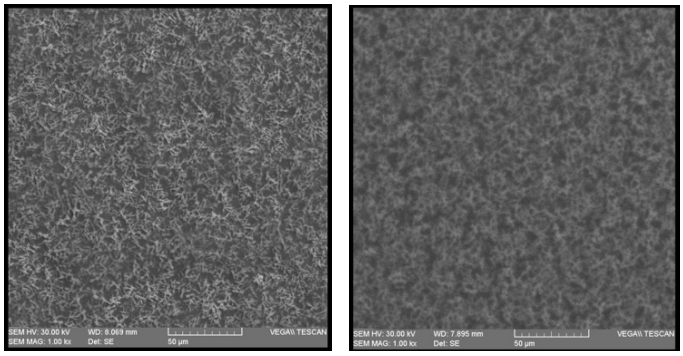

(a) (b)

Fig. 7. SEM-Top images of the perovskite surface with (a) PMMA, and (b) AZ5214 photoresist, in comparison with the perovskite surface in Fig. 6.

where the spin speed and solution concentration were carefully adjusted to achieve the desired thicknesses. The thickness of the PMMA layer was set at 127 nanometers, and the AZ5214 photoresist layer was set at 1200 nanometers. In terms of environmental protection, the PMMA and AZ5214 layers serve as effective barriers against moisture and other environmental factors. The PMMA layer, being thinner, offers a good level of protection but is limited by its lower thickness. On the other hand, the AZ5214 photoresist layer, being significantly thicker, provides superior protection. This enhanced protection is due to its ability to more effectively block moisture and environmental contaminants, which in turn helps to maintain the stability and performance of the perovskite layer over extended periods.

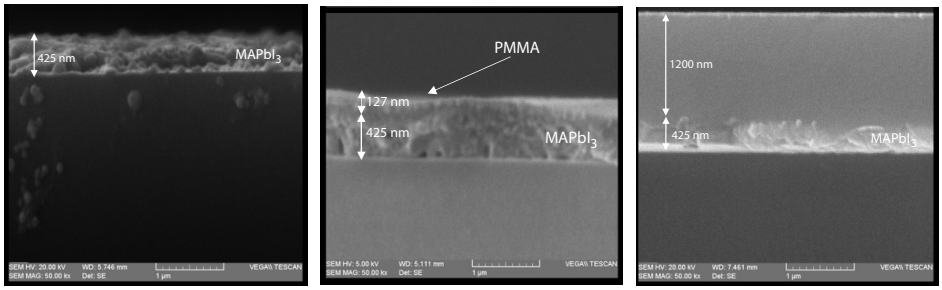

(a) (b) (c)

Fig. 8. Thickness comparison of (a) $MAPbI_3$ perovskite, (b) perovskite with PMMA, and (c) perovskite with AZ5214 photoresist.

3.2. X-ray diffraction (XRD) analysis

Figure 9 presents the X-ray diffraction (XRD) analysis of the perovskite phase of the $MAPbI_3$ film at two different time points: 24 hours and 40 days after deposition. This analysis aims to investigate the crystal structure and assess stability by comparing the obtained results with the XRD pattern from Ref. [40].

In Figure 10, XRD analysis of the perovskite film, along with AZ5214 photoresist, one day and 40 days after deposition is presented. According to the obtained diagram, there is no change observed after 40 days. The average grain size (D) of the $MAPbI_3$ nanocrystals can be calculated based on the (002) peak observed at 14.2° using the Scherrer equation. This equation relates

Optical Materials EXPRESS

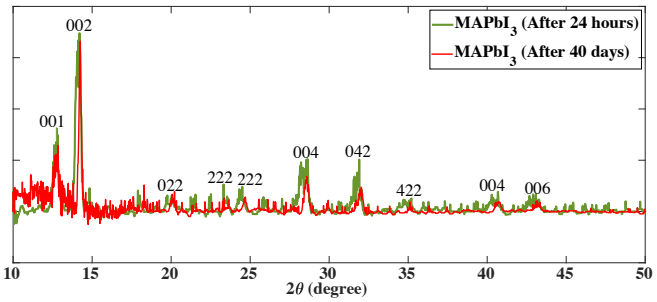

Fig. 9. X-ray diffraction (XRD) analysis of the perovskite film 24 hours and 40 days after deposition. Angles of 12.74°, 14.20°, 19.76°, 23.32°, 24.50°, 28.64°, 31.90°, 35.20°, and 42.90° correspond to the (001), (002), (022), (222), (004), (042), (422), (044), and (006) planes, respectively. A decrease in peak intensity is observed after 40 days.

the grain size to the wavelength of X-rays (λ), the Bragg diffraction angle (θ), the full width at half maximum (FWHM) of the (002) diffraction peak, and a constant factor (k). Specifically, the equation is expressed as $D = k\lambda/(\beta\cos(\theta))$, where k is the Scherrer constant (typically 0.89) and λ is the X-ray wavelength (0.154 nm). By applying this equation, one can accurately determine the average grain size of the nanocrystals. The FWHM of the (002) diffraction peak is 0.41, resulting in an average grain size of approximately 19 nanometers.

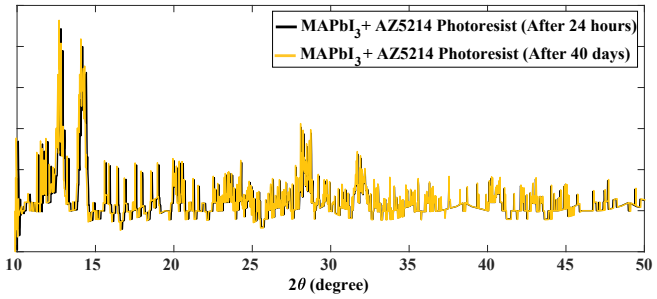

Fig. 10. X-ray diffraction (XRD) analysis of the perovskite film along with AZ5214 photoresist 24 hours and 40 days after deposition.

The consistent XRD patterns observed over a 40-day period underscore the structural integrity and stability of the $MAPbI_3$ perovskite films, even when integrated with AZ5214 photoresist. This stability, particularly in the absence of any significant structural changes over time, is indicative of a robust perovskite film. The calculated average grain size of 19 nanometers further validates the high-quality crystal structure of the $MAPbI_3$ nanocrystals within the film. The retention of crystal structure and grain size over an extended period highlights the effectiveness of our matrix encapsulation approach in preserving the structural attributes of the perovskite film. Such a stable and well-defined crystal structure is crucial for optoelectronic applications, as it directly impacts the material's optical and electronic properties. Therefore, the results presented here not only demonstrate the successful preparation of high-quality perovskite films but also affirm their potential longevity and performance in device applications. This alignment with the referenced XRD pattern from the literature further corroborates the high structural fidelity of our perovskite films, establishing a solid foundation for their application in stable and efficient optoelectronic devices.

Optical Materials EXPRESS

3.3. PL spectra analysis of $MAPbI_3$ and $MAPbBr_3$

Figures 11(a) to 11(f) depict the intensity of the PL spectra for $MAPbI_3$ and $MAPbBr_3$, respectively, showcasing optimized perovskite, perovskite with PMMA, and AZ5214 photoresist. To examine PL in the laboratory, we used a helium-neon laser, which emits spectra in the wavelength range of 450 to 540 nm. The emission of $MAPbI_3$, being in the range of 740 to 820 nm, does not interfere with the wavelength of the laser. However, the emission of $MAPbBr_3$ is approximately in the range of 520 to 580 nm, and we observe interference between the emission of $MAPbBr_3$ and the laser. This interference does not affect our examination results, and the peak shift is clearly observed. In the process of PL, electrons in the sample absorb energy from incident photons with energies higher than the bandgap of the electrons. As a result, electrons are excited to higher energy levels, and then they return to the ground state by emitting light again. Given that orthorhombic $MAPbI_3$ is a direct-band-gap crystal, the presence of multiple PL peaks signifies the involvement of various radiative recombination centers. These may include intrinsic defect states, extrinsic impurities, and residual tetragonal $MAPbI_3$ crystals. The deposition of PMMA and AZ5214 photoresist leads to a reduction in this red shift, which is one of the positive outcomes of this study. Figures 11(a) to 11(f) demonstrate that over time, the intensity of PL decreases for the optimized perovskite. However, after deposition with PMMA and AZ5214 photoresist, the decrease in PL intensity is less pronounced, indicating the stability of the perovskite layer. The $MAPbI_3$ perovskite with a 127-nanometer layer of PMMA resulted in a PL intensity retention of 44.8% after 40 days, which is a 589.23% improvement over the uncoated perovskite. Similarly, a 1200-nanometer layer of AZ5214 photoresist achieved a PL intensity retention of 38.2%, reflecting a 487.69% enhancement. For $MAPbBr_3$ perovskite, the PMMA coating achieved a PL intensity retention of 43.1%, a 71.72% improvement, while the AZ5214 coating resulted in a retention of 48.4%, showing a 92.83% enhancement. These findings highlight the superior stability provided by AZ5214 photoresist, especially for $MAPbBr_3$, making it a more effective barrier against environmental degradation compared to PMMA.

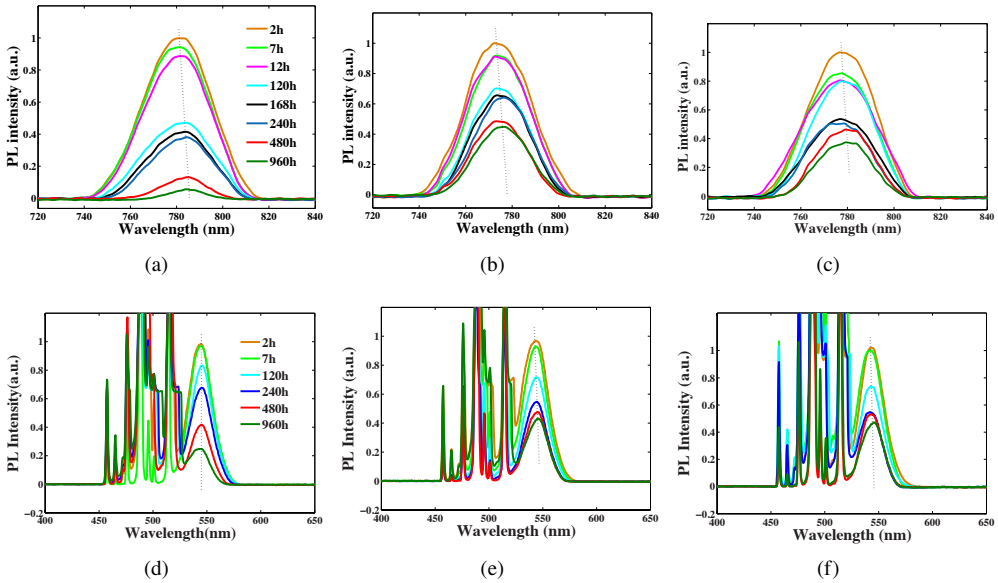

Fig. 11. PL spectra of (a) $MAPbI_3$ perovskite, (b) $MAPbI_3$ perovskite with PMMA, (c) $MAPbI_3$ perovskite with AZ5214 photoresist, (d) $MAPbBr_3$ perovskite, (e) $MAPbBr_3$ perovskite with PMMA, and (f) $MAPbBr_3$ perovskite with AZ5214 photoresist.

Optical Materials EXPRESS

In Figs. 12(a) to 12(d), the displacement of the peak center for the three states depicted in Figs. 11(a) to 11(f) has been investigated for $MAPbI_3$ and $MAPbBr_3$ perovskites, respectively. The black curve corresponds to the perovskite with the maximum displacement of the peak center. One of the positive outcomes of employing PMMA and AZ5214 photoresist is the reduction of this peak displacement towards the right. Among these options, AZ5214 Photoresist proves to be superior to PMMA. This superiority stems from its reduced moisture penetration into the perovskite, thereby resulting in less structural degradation. In fact, the absence or reduction of a rightward shift serves as an indication of layer stability. With the coating of AZ5214 photoresist and PMMA on $MAPbI_3$, the peak center shifts by approximately 4 and 6 nanometers, respectively. Additionally, the rightward shift of the peak center will decrease. With the coating of these two materials on $MAPbBr_3$ perovskite, the peak center shifts by approximately 2 nanometers (blue shift) and the shift amplitude is reduced. The positive results indicate that the use of AZ5214 photoresist and PMMA prevents shift, while the results related to AZ5214 photoresist are better than PMMA. The process of reducing the Full Width at Half Maximum (FWHM), the area under the curve, and the intensity with the coating of AZ5214 photoresist and PMMA on both perovskites decreases almost equally.

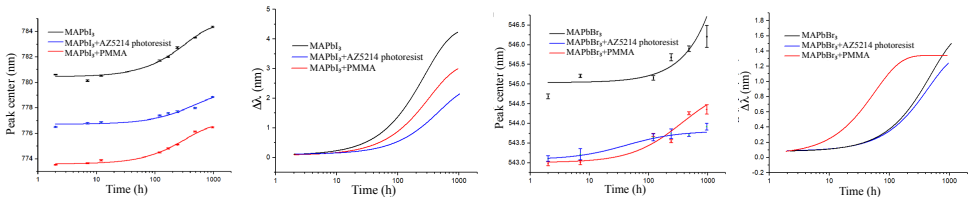

Fig. 12. Experimental results for peak center displacement and peak center displacement relative to the initial spectrum, i.e., $\Delta\lambda$. (a) peak center for $MAPbI_3$ perovskite, $MAPbI_3$ with AZ5214 photoresist, and $MAPbI_3$ with PMMA. (b) $\Delta\lambda$ for $MAPbI_3$ perovskite, $MAPbI_3$ with AZ5214 photoresist, and $MAPbI_3$ with PMMA. (c) peak center for $MAPbBr_3$ perovskite, $MAPbBr_3$ with AZ5214 photoresist, and $MAPbBr_3$ with PMMA. (d) $\Delta\lambda$ for $MAPbBr_3$ perovskite, $MAPbBr_3$ with AZ5214 photoresist, and $MAPbBr_3$ with PMMA.

When coatings of PMMA and AZ5214 photoresist are applied to $MAPbBr_3$ perovskite, the photoluminescence (PL) spectrum shows a blue shift of approximately 2 nanometers and a reduction in the shift amplitude. This observation can be explained through several mechanisms related to the interactions between the coatings and the perovskite material. The blue shift occurs due to the following reasons:

- Quantum confinement effect: Coatings like PMMA and AZ5214 photoresist can cause slight compression of the perovskite crystal structure. This compression may induce quantum confinement effects, where the spatial restriction of charge carriers increases their energy, resulting in a blue shift of the emission peak.
- Surface passivation: Both PMMA and AZ5214 photoresist act as surface passivating agents, reducing surface defects and trap states. By passivating these traps, the non-radiative recombination of charge carriers is minimized, leading to more efficient radiative recombination at higher energy levels, thus causing a blue shift.
- Stress and strain effects: The application of the coatings introduces mechanical stress or strain on the perovskite lattice. Compressive strain can lead to reduced interatomic distances and an increase in the material's bandgap, shifting the emission peak to shorter wavelengths (blue shift).

Optical Materials EXPRESS

- Reduction in defects and improved crystallinity: Coatings can improve the overall crystallinity of the perovskite by reducing surface defects. Improved crystallinity and fewer defects can result in fewer low-energy states within the bandgap, thereby shifting the emission peak towards higher energies (blue shift).

4. Discussion

The synthesized perovskite solutions, $MAPbI_3$ and $MAPbBr_3$, demonstrated efficient fabrication of thin films using the nanocrystal-pinning (NCP) process. Through SEM analysis, the morphology of the perovskite thin layer was elucidated, indicating successful encapsulation with PMMA and AZ5214 Photoresist without altering the inherent structure. This encapsulation process was further confirmed by XRD analysis, revealing enhanced stability of the perovskite layer, especially evident with AZ5214 Photoresist deposition. PL spectra analysis highlighted the sustained intensity of luminescence over time, emphasizing the role of PMMA and AZ5214 Photoresist in mitigating degradation. Importantly, the displacement of peak centers in the PL spectra indicated superior stability with AZ5214 Photoresist, attributable to its reduced moisture penetration and structural integrity. These findings underscore the novelty of utilizing AZ5214 Photoresist as a promising alternative for enhancing the durability and performance of perovskite-based optoelectronic devices.

The reduction in peak displacement towards the right when employing PMMA and AZ5214 photoresist suggests that these materials are effective in stabilizing the perovskite structure. This stabilization arises from their interaction with the perovskite material, influencing its properties and performance. Among PMMA (Polymethyl methacrylate) and AZ5214 photoresist, AZ5214 photoresist proves to be superior for several reasons:

- Chemical compatibility: AZ5214 exhibits better chemical compatibility with the perovskite material, enhancing surface passivation. This reduces defects and trap states in the perovskite, stabilizing the crystal structure and reducing peak displacement.
- Adhesion properties: AZ5214 provides better adhesion to the perovskite surface compared to PMMA. Stronger adhesion results in a more uniform and stable coating, protecting the perovskite from environmental degradation and ion migration, thereby reducing peak displacement.
- Moisture barrier: AZ5214 offers superior moisture barrier properties. Given the high sensitivity of perovskite materials to moisture, improved moisture resistance enhances the stability of the perovskite structure, further reducing peak displacement.
- Thermal stability: AZ5214 has better thermal stability than PMMA. Enhanced thermal stability prevents degradation of the perovskite material under thermal stress, contributing to reduced peak displacement.
- Electrical properties: The electronic properties of AZ5214 are more favorable for the perovskite interface, leading to better charge transport and reduced recombination losses, indirectly stabilizing the peak position.

Through our experimental investigations, we have demonstrated the effectiveness of matrix encapsulation in stabilizing perovskite thin films and prolonging their operational lifespan. Future research endeavors in this direction could explore novel encapsulating materials and deposition techniques to further enhance the performance and durability of perovskite-based devices for a wide range of applications in optoelectronics and beyond.

The thickness of the covering layer is directly influenced by the spin speed during the spin coating process. Our study aimed to optimize the hydrophobic barrier with the thinnest possible

Optical Materials EXPRESS

layer, which we achieved at approximately 1.2 microns using our spin coating device. This thickness was chosen to maximize the performance based on initial testing and feasibility within our experimental setup. While we acknowledge that varying thicknesses could affect hydrophobicity, our focus was to establish a baseline effectiveness rather than explore a range of thicknesses. Future investigations could explore the impact of different thicknesses on hydrophobic properties to further optimize performance.

5. Conclusions

In conclusion, we have demonstrated the efficacy of AZ5214 photoresist deposition for stabilizing perovskite layers. Through a comparative analysis with PMMA deposition, AZ5214 photoresist proved superior in enhancing the stability of the perovskite layer, particularly at a thickness of 1.2 microns, surpassing the stabilization achieved with PMMA at a thickness of 127 nanometers. Moreover, the self-assembly properties of AZ5214 photoresist confer resistance against heat and moisture, further establishing its superiority over PMMA. Our results demonstrate that the application of a 127-nanometer PMMA layer on $MAPbI_3$ perovskite leads to a remarkable 589.23% increase in stability, with a PL intensity retention of 44.8% after 40 days. The 1200-nanometer AZ5214 photoresist layer, while also significantly improving stability, achieves a PL intensity retention of 38.2%, reflecting a 487.69% improvement. For $MAPbBr_3$ perovskite, the enhancements were 71.72% for PMMA and 92.83% for AZ5214, with respective PL intensity retentions of 43.1% and 48.4%. These substantial improvements underscore the efficacy of AZ5214 photoresist in enhancing perovskite stability, particularly in providing a robust barrier against environmental factors, thus offering a promising solution for the long-term durability of perovskite-based optoelectronic devices. These findings underscore the potential of AZ5214 photoresist as a promising candidate for enhancing the durability and performance of perovskite-based devices in various optoelectronic applications.

Disclosures. The authors declare no conflicts of interest.

Data availability. The data that supports the findings of this study is available from the corresponding author upon reasonable request.

References

1. Z. Wang, S. Shu, X. Wei, *et al.*, "Flexophotovoltaic effect and above-band-gap photovoltage induced by strain gradients in halide perovskites," Phys. Rev. Lett. **132**(8), 086902 (2024).
2. A. C. Ferreira, A. Létoublon, S. Paofai, *et al.*, "Elastic softness of hybrid lead halide perovskites," Phys. Rev. Lett. **121**(8), 085502 (2018).
3. D. W. de Quilettes, S. M. Vorpahl, S. D. Stranks, *et al.*, "Impact of microstructure on local carrier lifetime in perovskite solar cells," Science **348**(6235), 683–686 (2015).
4. N. J. Jeon, H. Na, E. H. Jung, *et al.*, "A fluorene-terminated hole-transporting material for highly efficient and stable perovskite solar cells," Nat. Energy **3**(8), 682–689 (2018).
5. T. M. Brenner, D. A. Egger, L. Kronik, *et al.*, "Hybrid organic-inorganic perovskites: low-cost semiconductors with intriguing charge-transport properties," Nat. Rev. Mater. **1**(1), 15007 (2016).
6. P. Qin, S. Tanaka, S. Ito, *et al.*, "Inorganic hole conductor-based lead halide perovskite solar cells with 12.4% conversion efficiency," Nature communications **5**(1), 3834 (2014).
7. P. Basera, M. Kumar, S. Saini, *et al.*, "Reducing lead toxicity in the methylammonium lead halide mapbi$_3$: Why sn substitution should be preferred to pb vacancy for optimum solar cell efficiency," Phys. Rev. B **101**(5), 054108 (2020).
8. T. J. Whitcher, J.-X. Zhu, X. Chi, *et al.*, "Importance of electronic correlations and unusual excitonic effects in formamidinium lead halide perovskites," Phys. Rev. X **8**(2), 021034 (2018).
9. Q. A. Akkerman, G. Rainò, M. V. Kovalenko, *et al.*, "Genesis, challenges and opportunities for colloidal lead halide perovskite nanocrystals," Nat. Mater. **17**(5), 394–405 (2018).
10. S. D. Stranks and H. J. Snaith, "Metal-halide perovskites for photovoltaic and light-emitting devices," Nat. Nanotechnol. **10**(5), 391–402 (2015).
11. S. Taravati and G. V. Eleftheriades, "Generalized space-time-periodic diffraction gratings: Theory and applications," Phys. Rev. Appl. **12**(2), 024026 (2019).
12. S. Taravati and G. V. Eleftheriades, "Full-duplex nonreciprocal beam steering by time-modulated phase-gradient metasurfaces," Phys. Rev. Appl. **14**(1), 014027 (2020).
13. S. Taravati and G. V. Eleftheriades, "Full-duplex reflective beamsteering metasurface featuring magnetless nonreciprocal amplification," Nat. Commun. **12**(1), 4414 (2021).

Optical Materials EXPRESS

14. S. Taravati and G. V. Eleftheriades, "Microwave space-time-modulated metasurfaces," ACS Photonics **9**(2), 305–318 (2022).
15. K. As'ham, I. Al-Ani, W. Lei, *et al.*, "Mie exciton-polariton in a perovskite metasurface," Phys. Rev. Appl. **18**(1), 014079 (2022).
16. F. Ye, H. Chen, F. Xie, *et al.*, "Soft-cover deposition of scaling-up uniform perovskite thin films for high cost-performance solar cells," Energy Environ. Sci. **9**(7), 2295–2301 (2016).
17. T. Li, X. Zhao, D. Yang, *et al.*, "Intrinsic defect properties in halide double perovskites for optoelectronic applications," Phys. Rev. Appl. **10**(4), 041001 (2018).
18. X. Hu, H. Wang, M. Wang, *et al.*, "Interfacial defects passivation using fullerene-polymer mixing layer for planar-structure perovskite solar cells with negligible hysteresis," Sol. Energy **206**, 816–825 (2020).
19. C. Gong, H. Li, H. Wang, *et al.*, "Silver coordination-induced n-doping of PCBM for stable and efficient inverted perovskite solar cells," Nat. Commun. **15**(1), 4922 (2024).
20. K. Wang, Z. Xu, Z. Guo, *et al.*, "Phosphonate diacid molecule induced crystallization manipulation and defect passivation for high-performance inverted MA-free perovskite solar cells," Advanced Energy Materials **1**, 2402249 (2024).
21. C. Zhang, H. Li, C. Gong, *et al.*, "Crystallization manipulation and holistic defect passivation toward stable and efficient inverted perovskite solar cells," Energy Environ. Sci. **16**(9), 3825–3836 (2023).
22. M. A. Green, A. Ho-Baillie, and H. J. Snaith, "The emergence of perovskite solar cells," Nat. Photonics **8**(7), 506–514 (2014).
23. A. Akhanuly, I. T. Dossyaev, E. O. Shalenov, *et al.*, "Modeling and comparative performance analysis of perovskite solar cells with planar or nanorod sno_2 electron-transport layers," Phys. Rev. Appl. **19**(5), 054039 (2023).
24. L. Jiang, R. Liu, R. Su, *et al.*, "Continuous wave pumped single-mode nanolasers in inorganic perovskites with robust stability and high quantum yield," Nanoscale **10**(28), 13565–13571 (2018).
25. J. Xing, Y. Zhao, M. Askerka, *et al.*, "Color-stable highly luminescent sky-blue perovskite light-emitting diodes," Nat. Commun. **9**(1), 3541 (2018).
26. R. Chakraborty, G. Paul, and A. J. Pal, "Quantum confinement and dielectric deconfinement in quasi-two-dimensional perovskites: their roles in light-emitting diodes," Phys. Rev. Appl. **17**(5), 054045 (2022).
27. M. Nabi, S. S. Padelkar, J. J. Jasieniak, *et al.*, "Lead-free magnetic double perovskites for photovoltaic and photocatalysis applications," Phys. Rev. Appl. **21**(1), 014063 (2024).
28. M. I. Saidaminov, V. Adinolfi, R. Comin, *et al.*, "Planar-integrated single-crystalline perovskite photodetectors," Nat. Commun. **6**(1), 8724 (2015).
29. B. Wang, X. Yang, R. Li, *et al.*, "One-dimensional $CsCu_2I_3$ single-crystal x-ray detectors," ACS Energy Lett. **8**(10), 4406–4413 (2023).
30. T. Leijtens, G. E. Eperon, N. K. Noel, *et al.*, "Stability of metal halide perovskite solar cells," Advanced Energy Materials **5**, 1500963 (2015).
31. T. A. Berhe, W.-N. Su, C.-H. Chen, *et al.*, "Organometal halide perovskite solar cells: degradation and stability," Energy Environ. Sci. **9**(2), 323–356 (2016).
32. D. Wang, M. Wright, N. K. Elumalai, *et al.*, "Stability of perovskite solar cells," Sol. Energy Mater. Sol. Cells **147**, 255–275 (2016).
33. S. Guarnera, A. Abate, W. Zhang, *et al.*, "Improving the long-term stability of perovskite solar cells with a porous Al_3O_3 buffer layer," J. Phys. Chem. Lett. **6**(3), 432–437 (2015).
34. S. Huang, Z. Li, L. Kong, *et al.*, "Enhancing the stability of $CH_3NH_3PbBr_3$ quantum dots by embedding in silica spheres derived from tetramethyl orthosilicate in waterless toluene," J. Am. Chem. Soc. **138**(18), 5749–5752 (2016).
35. D. Di, K. P. Musselman, G. Li, *et al.*, "Size-dependent photon emission from organometal halide perovskite nanocrystals embedded in an organic matrix," J. Phys. Chem. Lett. **6**(3), 446–450 (2015).
36. R. Tannenbaum, M. Zubris, K. David, *et al.*, "FTIR characterization of the reactive interface of cobalt oxide nanoparticles embedded in polymeric matrices," J. Phys. Chem. B **110**(5), 2227–2232 (2006).
37. R. Tannenbaum, S. King, J. Lecy, *et al.*, "Infrared study of the kinetics and mechanism of adsorption of acrylic polymers on alumina surfaces," Langmuir **20**(11), 4507–4514 (2004).
38. D. Ciprari, K. Jacob, and R. Tannenbaum, "Characterization of polymer nanocomposite interphase and its impact on mechanical properties," Macromolecules **39**(19), 6565–6573 (2006).
39. X. Li, Z. Xue, D. Luo, *et al.*, "A stable lead halide perovskite nanocrystals protected by pmma," Sci. China Mater. **61**(3), 363–370 (2018).
40. H. Wei, Y. Tang, B. Feng, *et al.*, "Importance of PbI_3 morphology in two-step deposition of $CH_3NH_3PbI_3$ for high-performance perovskite solar cells," Chinese Physics B **26**(12), 128801 (2017).
41. R. Guo, M. V. Khenkin, G. E. Arnaoutakis, *et al.*, "Initial stages of photodegradation of $MAPbI_3$ perovskite: accelerated aging with concentrated sunlight," Solar RRL **4**(2), 1900270 (2020).
42. A. A. Melvin, V. D. Stoichkov, J. Kettle, *et al.*, "Lead iodide as a buffer layer in UV-induced degradation of $CH_3NH_3PbI_3$ films," Sol. Energy **159**, 794–799 (2018).